AIAA JOURNAL
Vol. 45, No. 8, August 2007

Fluid-Dynamics-Based Analytical Model for Synthetic Jet Actuation

Rajnish N. Sharma*
University of Auckland, Auckland 1010, New Zealand

DOI: 10.2514/1.25427

An analytical model for synthetic jet actuation based on the laws of fluid dynamics is presented. A synthetic jet actuator consists of a cavity with a driven wall and an orifice. Under actuation, the wall is oscillated, resulting in an oscillatory flow through the orifice. In the model, the driven wall is modeled as a single-degree-of-freedom mechanical system, which is pneumatically coupled to the cavity–orifice arrangement acting as a Helmholtz resonator. The latter was modeled using the unsteady form of the continuity and Bernoulli equations with a loss term. The model was validated against experimental data available in the published literature, and very good agreement is obtained between the predicted and measured frequency responses as well as for the phase relationships between velocities and pressures. The model and analysis based on it provide valuable insights into the behavior of synthetic jet actuators and reveal that air in the actuator cavity exhibits compressibility at all frequencies beyond the Helmholtz resonance frequency.

Nomenclature

A_o	=	orifice area
A_w	=	wall area
C_c	=	orifice contraction coefficient
C_d	=	discharge coefficient
C_I	=	inertia coefficient
C_L	=	sudden-flow-contraction loss coefficient
c_a	=	added diaphragm damping coefficient
c_w	=	diaphragm damping coefficient
c_{wt}	=	$c_w + c_a$
D_a	=	effective acoustic piezoelectric coefficient when uncoupled from actuator cavity, $\Delta V/v_a$
d_o	=	orifice diameter
d_w	=	diaphragm/wall diameter
f	=	frequency
f_h	=	Helmholtz resonance frequency
f_w	=	diaphragm/wall natural frequency
F	=	force
F_a	=	force amplitude
K	=	orifice loss coefficient
k_h	=	stiffness of orifice air against the cavity
k_w	=	diaphragm/wall stiffness
k_{wp}	=	pneumatic stiffness of the diaphragm against the sealed actuator cavity, $\gamma A_w^2 P_o/V_o$
L	=	length
L_c	=	characteristic length of the actuator
l_e	=	effective length of the air jet/slug
l_o	=	orifice length (thickness)
m_a	=	added diaphragm/wall mass
m_h	=	mass of the air jet at the orifice, $\rho_a A_o l_e$
m_w	=	diaphragm/wall mass
m_{wt}	=	$m_w + m_a$
n	=	polytropic exponent
P_i	=	$p_i + P_o$
P_o	=	ambient pressure
p_i	=	gauge internal pressure
p_{io}	=	steady gauge internal pressure
U	=	orifice flow velocity
U_o	=	steady orifice jet velocity
U_S	=	speed of sound
U_{vc}	=	velocity at the region of vena contracta near the orifice
U_w	=	wall velocity
V	=	instantaneous cavity volume
V_o	=	nominal cavity volume
v	=	input voltage
v_a	=	amplitude of input voltage
x_w	=	wall displacement
Z_a	=	characteristics of the actuation mechanism
γ	=	specific heat ratio
ΔV	=	volume displaced by the diaphragm
ε	=	velocity ratio, U_{vc}/U
λ	=	wavelength
ρ_a	=	ambient air density
ρ_i	=	internal air density
ρ_i'	=	internal air density perturbation
ζ_w	=	diaphragm/wall damping ratio
$\phi_{P_i\text{-}U}$	=	phase angle between the actuator internal pressure and orifice flow velocity
$\phi_{V_w\text{-}U}$	=	phase angle between the diaphragm and orifice flow velocities
ω	=	$2\pi f$
ω_h	=	$2\pi f_h$
ω_w	=	$2\pi f_w$
ω_{wp}	=	$\sqrt{k_{wp}/m_{wt}}$

Presented as Paper 3035 at the 3rd AIAA Flow Control Conference, San Francisco, CA, 5–8 June 2006; received 25 May 2006; revision received 31 March 2007; accepted for publication 6 April 2007.

*Senior Lecturer, Department of Mechanical Engineering, Private Bag 92019; r.sharma@auckland.ac.nz. Member AIAA.

I. Introduction

A SYNTHETIC JET is a quasi-steady jet of air generated a few diameters from the orifice of a synthetic jet actuator, as illustrated in Fig. 1. Actuation involves the forcing of an oscillatory airflow through the orifice from a cavity with a driven flexible wall [1]. During outflow, an air jet is formed directly in front of the orifice, accompanied by a vortex ring around the orifice, which is shed as outflow weakens and reverts to inflow. Because the inflow part of the oscillatory cycle entrains air from around the shed vortex ring, the flowfield established some distance downstream of the orifice is relatively undisturbed and the shed vortices are not destructed, leading to the maintenance of a quasi-steady or synthetic jet. The train of vortex rings that are periodically shed and advected away from the orifice eventually break down in the region of this synthetic jet, thus intermittently transporting momentum to and thereby

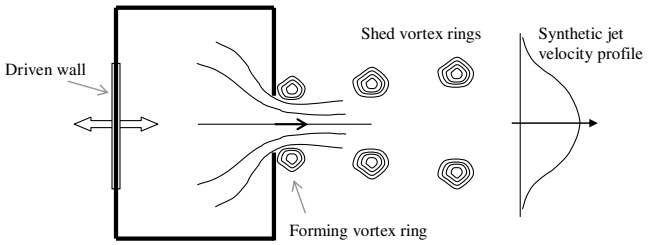

Fig. 1 Synthetic jet actuator.

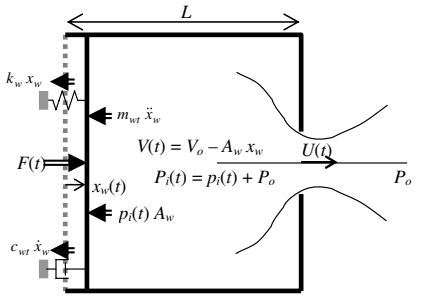

Fig. 2 Schematic of the synthetic jet.

sustaining the jet [2]. A major advantage of the synthetic jet over the ordinary steady jet is that it does not require a continuous supply of fluid from elsewhere for the maintenance of the jet, because the air jet is synthesized from the surrounding fluid. Consequently, the actuator has advantages of simple structure, low cost, and easy installation. The synthetic jet has thus attracted much research within the last decade and a comprehensive review will be found in Glezer and Amitay [3]. Past investigations into applications of synthetic jets range from thrust vectoring of jet engines [4], through mixing enhancement [5], to external flow boundary-layer separation control [6]. A number of studies (for example, Smith [7]), have focused upon the interaction of synthetic jets with boundary-layer crossflows. Benchiekh et al. [8] and Amitay et al. [9] attempted the control of separation in internal flows (in particular, inside a diffuser) with some measure of success. Synthetic jets have also been used to enhance heat and mass transfer [10,11].

Although understanding of the evolution and characteristics of synthetic jets is important in the development of its applications, the actuation and optimization of actuators are equally as important. Mallinson et al. [12] showed that the resultant jet shows evidence of the influence of acoustic resonance of the cavity and structural resonance of the flexible wall. Guy et al. [13,14] showed that the output of the actuator is maximized at the two resonance frequencies. Furthermore, it is suggested that there is an optimum combination of all geometric parameters at which the actuator will operate at its full capacity. Gallas et al. [15–17] offered a lumped element model (LEM) based upon an analogy with electrical circuitry, in which the components of a piezoelectrically driven synthetic jet actuator are modeled as elements of an equivalent electrical circuit. Gallas et al. discussed methods of estimation of model parameters and provided experimental verification of their model. Agreement between the model and experimental data was found to be good, allowing some measure of optimization of the actuator. Gallas et al. [18] also found that the actuator orifice flow is characterized by linear and nonlinear losses, depending upon oscillating-wall stroke lengths relative to the orifice size; however, they conclude that further investigation is required to develop correlations for orifice loss coefficients as functions of Reynolds number and wall stroke lengths.

The purpose of this paper is to present an alternative synthetic jet actuation model based on the laws of fluid dynamics, capable of additionally predicting cavity internal pressure fluctuations and the phase relationships between the different variables. Furthermore, the model is then to be used for improving the understanding of the performance of the actuator and its sensitivity to changes of important design parameters.

II. Development of the Model

The problem to be considered is the actuation of the cavity wall of a typical synthetic jet actuator through an input supply voltage, as illustrated in the schematic of Fig. 2. The actuator is assumed to interact with quiescent air. We are interested in deriving a relationship between the output of the actuator [namely, the orifice flow velocity $U(t)$], as well as the actuator cavity internal pressure $p_i(t)$, and the driving force $F(t)$ effected through an input voltage $v(t)$. We assume at this stage that $F(t)$ is some known function of $v(t)$ and the characteristics of the actuation mechanism Z_a

$$F(t) = g[v(t), Z_a] \tag{1}$$

The oscillating wall could take one of a number of different forms, such as a piezoelectrically driven diaphragm, mechanically driven piston, or mechanically driven diaphragm. For example, $F(t)$ could be an electrodynamic force generated with varying input voltage $v(t)$, such as that in an audio-speaker mechanism.

For simplicity, we consider the flexible wall behaving as a piston and it is deemed to displace as a rigid body in one dimension. An audio speaker displays such a behavior in the middle- to low-frequency range (Kinsler et al. [19] p. 410) because the speed of transverse waves is about 500 m/s. Consequently, it is reasonable to assume that the speaker cone moves as a unit for frequencies below 500 Hz. From a mechanical systems point of view, a piezoelectrically driven diaphragm displays behavior similar to that of a single-degree-of-freedom system [15–17]. In this way, the driven wall of a synthetic jet actuator is readily modeled as a mechanical mass-damper-stiffness system having a mass m_w, damping coefficient c_w, and stiffness k_w. An added mass term m_a representing added air mass would be significant if the diaphragm or driven wall is lightweight. In addition, an acoustic radiation damping force $c_a\dot{x}_w$ could be expected. Under actuation, the gauge pressure inside the cavity $p_i(t)$ will fluctuate about a zero mean value as the air undergoes compression and expansion. Consequently, an equation governing the dynamics of the flexible membrane may thus be obtained under the action of the electromotive and internal pressure forces as

$$m_{\mathrm{wt}}\ddot{x}_w + c_{\mathrm{wt}}\dot{x}_w + k_w x_w = F - p_i A_w \tag{2a}$$

in which $A_w = \pi d_w^2/4$ is the area of the flexible wall, $x_w(t)$ is its displacement, and m_{wt} and c_{wt} are the total mass ($m_{wt} = m_w + m_a$) and damping coefficient ($c_{wt} = c_w + c_a$).

For a circular piston vibrating in an infinite baffle at cyclic frequency f or radian frequency $w = 2\pi f$, the added mass and damping terms are (Kinsler et al. [19])

$$m_a = \rho_a A_w U_S X_1(y)/\omega, \qquad c_a = \rho_a A_w U_S R_1(y) \tag{2b}$$

where the functions $X_1(y)$ and $R_1(y)$ are defined in terms of the Struve function of the first kind $H_1(y)$ and the first-order Bessel function of the first kind $J_1(y)$, respectively, as follows:

$$y = \omega\,\mathrm{d}_w/U_S \tag{2c}$$

$$X_1(y) = 2\boldsymbol{H}_1(y)/y = (4/\pi)[y/3 - y^3/(3^2\cdot 5) + y^5/(3^2\cdot 5^2\cdot 7) - \cdots] \tag{2d}$$

$$R_1(y) = 1 - 2J_1(y)/y = y^2/(2\cdot 4) - y^4/(2\cdot 4^2\cdot 6) + y^6/(2\cdot 4^2\cdot 6^2\cdot 8) - \cdots \tag{2e}$$

for $y < 1$. For a small actuator having a 10-mm-diam diaphragm operating in ambient conditions, the $y < 1$ restriction on Eqs. (2d) and (2e) means that these will give converged results for frequencies below approximately 5.5 kHz. Synthetic jet actuators are typically operated below this frequency (see, for example, Gallas et al. [15–17]).

Equation (2a) may be rewritten as

$$\ddot{x}_w + 2\varsigma_w\omega_w\dot{x}_w + \omega_w^2 x_w = F/m_{wt} - p_i A_w/m_{wt} \tag{3}$$

in which

$$\varsigma_w = c_{wt}/2\sqrt{m_{wt}k_w} \tag{4}$$

and

$$\omega_w = \sqrt{k_w/m_{wt}} = 2\pi f_w \tag{5}$$

These parameters will depend upon the structural characteristics of the wall and the manner in which it is supported.

If the wall is now oscillated, then the air inside the cavity will alternately undergo compression and expansion. This will be accompanied by an oscillatory flow through the orifice. The internal pressure in the cavity can be considered to be uniform (except close to the opening) at any given instant in time, provided that the wavelength λ of the pressure oscillations is much greater than a typical dimension L_c of the actuator cavity (i.e., provided that the frequency for the biggest standing wave of quarter-wavelength is well beyond the operating frequency range of the actuator). This requirement (see, for example, Hall [20]) can be expressed as

$$\lambda \equiv 2\pi U_S/\omega = U_S/f \gg L_c \tag{6}$$

where $U_S = \sqrt{(\gamma P_o/\rho_a)}$ is the speed of sound. For air at standard conditions, U_S is approximately 343 m/s and the criteria for the assumption of uniform internal pressure for three typical situations are summarized in Table 1. It is clear that for a miniature-scale model, this assumption may be justified for frequencies of actuation up to well over 30 kHz. When the preceding assumption is justified, then the instantaneous density of the bulk of the internal air can be expressed as the sum of a mean component and a fluctuating component as

$$\rho_i = \rho_a + \rho_i' \tag{7}$$

If the amplitude of oscillations of the flexible wall are much smaller than the length of the actuator (i.e., if $|x_w| \ll L$), then the physical volume of the cavity

$$V = V_o - A_w x_w \tag{8}$$

will suffer relatively small fluctuations $\Delta V = A_w x_w$, compared with the nominal volume V_o (i.e., $\Delta V \ll V_o$). Because air can flow out of and in through the orifice as well, then $\rho_i' \ll \rho_a$ (i.e., density changes are relatively small compared with its mean value). When this holds, application of the compressible form of the continuity equation to the air contained within gives

$$\mathrm{d}\,m_i/\mathrm{d}t = \mathrm{d}(\rho_i V)/\mathrm{d}t \approx V_o(\mathrm{d}\rho_i/\mathrm{d}t) - \rho_a A_w\dot{x}_w = -\rho_a A_o U \tag{9}$$

where m_i is the mass of air in the cavity and U is the air velocity in the plane of the orifice.

The bulk behavior of the air within the cavity may be assumed to follow a polytropic process. Assuming that the initial internal pressure equaled the ambient pressure P_o, we can express the relationship between instantaneous internal pressure and instantaneous density as

$$P_i/\rho_i^n = P_o/\rho_a^n \tag{10}$$

in which n is the polytropic exponent, which is equal to one for an isothermal process and equal to the specific heat ratio γ for an isentropic process. In their study, Rathnasingham and Breuer [21] assumed isothermal behavior, however, based on related studies [22–25], a more correct approach would be to assume that air undergoes isentropic contractions and expansions in the cavity. Thus,

$$\mathrm{d}\,\rho_i/\mathrm{d}t \approx (\mathrm{d}P_i/\mathrm{d}t)/(\gamma P_o/\rho_a) \tag{11}$$

because

$$\mathrm{d}\,P_i/\mathrm{d}t = \mathrm{d}(p_i + P_o)/\mathrm{d}t = \mathrm{d}p_i/\mathrm{d}t \tag{12}$$

the continuity equation (9) can now be rewritten as

$$V_o(\mathrm{d}p_i/\mathrm{d}t)/(\gamma P_o) - A_w\dot{x}_w = -A_o U \tag{13}$$

Now consider an outflow part of the cycle, as illustrated in Fig. 3a. The unsteady form of the Bernoulli equation may be applied between a point far enough upstream of the orifice, inside the cavity in which the flow velocity is negligible (i.e., much smaller than the orifice flow velocity), and a point at the vena contracta, outside the orifice, for which the velocity may be expressed as

$$U_{\mathrm{vc}} = \frac{A_o}{A_{\mathrm{vc}}}U = \frac{1}{C_c}U \tag{14}$$

In Eq. (14), C_c is a contraction coefficient representing the area ratio A_{vc}/A_o, which will vary according to the characteristic and strength of the vena contracta. At the vena contracta, the pressure is ambient and the losses can be quantified with a sudden-contraction minor loss coefficient C_L applied to the orifice flow dynamic pressure. Inclusion of this in the unsteady Bernoulli equation leads to

$$P_i = P_o + \tfrac{1}{2}\rho_a U_{\mathrm{vc}}^2 + C_L\tfrac{1}{2}\rho_a U^2 + \rho_a l_e(\mathrm{d}U/\mathrm{d}t) \tag{15a}$$

which is readily rewritten as

$$p_i = \left(C_L + \frac{1}{C_c^2}\right)\frac{1}{2}\rho_a U^2 + \rho_a l_e(\mathrm{d}U/\mathrm{d}t) \tag{15b}$$

For an inflow part of the cycle, as shown in Fig. 3b, and assuming that loss and discharge coefficients are similar to those during outflow, we similarly obtain

$$p_i = -\left(C_L + \frac{1}{C_c^2}\right)\frac{1}{2}\rho_a U^2 + \rho_a l_e(\mathrm{d}U/\mathrm{d}t) \tag{16}$$

Noting from Fig. 2 that U is positive for outflow and negative for inflow, Eqs. (15) and (16) may be combined into a single equation:

$$p_i = \left(C_L + \frac{1}{C_c^2}\right)\frac{1}{2}\rho_a |U|U + \rho_a l_e(\mathrm{d}U/\mathrm{d}t) \tag{17}$$

It should be noted that C_L represents the losses due to the sudden contraction of flow and is therefore different from the loss coefficient K quoted in texts for orifice plates and flow meters [see Eqs. (18a–18c)]. Under steady conditions, Bernoulli obstruction theory (see White [26] pp. 398–402) can be used to show that

Table 1 Criteria for uniform internal pressure

Description	Length scale L_c	Criteria
Bench-top	<0.50 m	$f < 680$ Hz
Pocket	<0.05 m	$f < 6.8$ kHz
Miniature	<0.01 m	$f < 34$ kHz

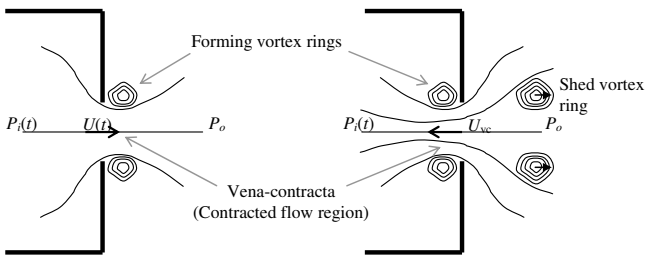

a) Outflow **b) Inflow**

Fig. 3 Orifice flow situations.

$$A_{vc}U_{vc} = A_oU = A_o \times \frac{C_d}{(1-\beta^4)^{1/2}}\left(\frac{2\Delta p}{\rho}\right)^{1/2} \tag{18a}$$

$$\Delta p = \tfrac{1}{2}\rho\left(U_{vc}^2 - 0^2\right) + C_L\tfrac{1}{2}\rho U^2 = K\tfrac{1}{2}\rho U^2 \tag{18b}$$

$$\frac{1}{C_c^2} = K - C_L = \frac{1-\beta^4}{C_d^2} - C_L \tag{18c}$$

in which C_d is the orifice discharge coefficient for flow through the orifice of area A_o, and $\beta = d_o/d_w = \sqrt{(A_o/A_w)}$. For a small β ratio, the steady value for C_d is approximately 0.6, whereas the loss coefficient C_L could be approximated as that for a sudden contraction (e.g., 0.42 for a very small β ratio; see White [26] p. 373).

In the present problem, however, the flow is unsteady and, in particular, sinusoidal about zero mean. The discharge coefficient C_d will therefore vary cyclically. Unfortunately, detailed data for such unsteady situations are not available, although various authors [20,22] have shown that the steady flow value of 0.6 works well under certain unsteady conditions, and it could be as high as 0.88.

Values for the effective length l_e may be estimated using data available in the acoustics literature (see, for example, Hall [20]) or from studies on building internal pressure dynamics induced through dominant openings [23–25]. The effective length of the air jet/slug at the orifice is a sum of the actual orifice length l_o and end corrections quantified using an inertia coefficient C_I [24], such that

$$l_e = l_o + C_I\sqrt{A_o} \tag{19}$$

It should be noted that Rathnasingham and Breuer [21] used an arbitrary value of $l_e = 2 \cdot d_o$.

Loss-coefficient data for steady flow situations are readily available from texts on fluid mechanics; however, the orifice flow under consideration is time-varying, and data are scarce. Vickery [24] concluded from his studies on building cavity excitation through orifice-type openings that in spite of the unsteady nature of the orifice flow, a constant value reflective of the steady flow situation nevertheless yields acceptable results. The sudden contraction and thin-orifice-plate loss coefficients (see, for example, White [26]) are given by

$$C_L = 0.42(1-\beta^2), \qquad K = \frac{1-\beta^4}{C_d^2} \tag{20}$$

Although the preceding parameter estimates might be reasonable under certain conditions, a more rigorous approach may be taken along the lines suggested in [15–17], which is based on information in [27].

Equations (13) and (17) may now be combined. First, however, given that there are indeed three ill-defined parameters [namely, l_e (or C_I), C_L, and C_c] and that the contraction ratio C_c appears in the damping or loss term only, we readily recognize that

$$C_L + \frac{1}{C_c^2} = K \tag{21}$$

If the orifice flow velocity U is eliminated, then an equation governing the dynamics of internal pressure is obtained:

$$\begin{aligned}&\ddot{p}_i + V_oK/(2\gamma A_oP_ol_e)|\dot{p}_i\\ &\quad - (\gamma A_wP_o/V_o)\dot{x}_w|[\dot{p}_i - (\gamma A_wP_o/V_o)\dot{x}_w] + \omega_h^2p_i\\ &\quad = (\gamma A_wP_o/V_o)\ddot{x}_w\end{aligned} \tag{22a}$$

$$\begin{aligned}&\ddot{p}_i + V_oK/(2\gamma A_oP_ol_e)|\dot{p}_i\\ &\quad - (m_w\omega_{\mathrm{wp}}^2/A_w)\dot{x}_w|[\dot{p}_i - (m_w\omega_{\mathrm{wp}}^2/A_w)\dot{x}_w] + \omega_h^2p_i\\ &\quad = (m_w\omega_{\mathrm{wp}}^2/A_w)\ddot{x}_w\end{aligned} \tag{22b}$$

However, if we chose to eliminate internal pressure p_i then an equation governing the dynamics of the mean orifice flow velocity is obtained:

$$\ddot{U} + (K/l_e)|U|\dot{U} + \omega_h^2U = [\gamma A_wP_o/(\rho_al_eV_o)]\dot{x}_w \tag{23a}$$

$$\ddot{U} + (K/l_e)|U|\dot{U} + \omega_h^2U = (A_w/A_o)\omega_h^2\dot{x}_w \tag{23b}$$

In Eqs. (22) and (23),

$$\begin{aligned}\omega_h = 2\pi f_h &= \sqrt{k_h/m_h} = \sqrt{\left(\gamma A_o^2P_o/V_o\right)\Big/(\rho_al_eA_o)}\\ &= \sqrt{(\gamma A_oP_o)/(\rho_al_eV_o)} = U_S\sqrt{A_o/(l_eV_o)}\end{aligned} \tag{24}$$

is the Helmholtz resonance frequency of the cavity with the orifice, and

$$\omega_{wp} = \sqrt{k_{wp}/m_w} = \sqrt{\left(\gamma A_w^2P_o/V_o\right)\Big/m_w} \tag{25}$$

is the natural frequency of the pneumatic spring made of the oscillatory wall of mass m_w against a sealed cavity volume V_o. Equations (22) and (23) are readily recognized as those for a Helmholtz acoustic resonator, but with pneumatic coupling to the dynamics of the oscillating wall. The synthetic jet actuator may therefore be viewed as a coupled mechanical (dynamic wall)–Helmholtz resonator system with two degrees of freedom. This fourth-order nature of the synthetic jet actuator has been discussed previously (see, for example, Gallas et al. [16]). If we take this view, then a number of deductions are possible. The actuation system will have two resonance modes, and it is possible to maximize the output velocity U if the actuator is driven near the resonance frequencies. It might also be possible to tune the actuator by adjusting either the Helmholtz frequency f_h or the wall resonance frequencies f_w. In this regard, the geometrical properties of the actuator are important in two ways. First, they directly determine the Helmholtz resonance frequency [see Eq. (24)], and second, they have an influence on the damping of the system. Examining Eqs. (22–24) reveals that a decrease in actuator cavity volume V_o will increase f_h (which will be of significant benefit if $f_h < f_w$) and will also decrease the damping. The same effects are also obtained with an increase in size of the orifice A_o; however, although the energy efficiency of the system will be improved, the output velocity will decrease, which may not be desirable from the point of view of the evolution of the synthetic jet.

For very low frequencies, or rather for the wall moving steadily at a velocity $\dot{x}_w = U_w$ (positive inwards and negative outwards from the cavity), the corresponding steady values for the orifice velocity U_o and the internal pressure p_{io} can be obtained from Eqs. (22) and (23) by setting time derivatives of U and p_i to zero, giving

$$U_o = (A_w/A_o)U_w \tag{26}$$

$$p_{\mathrm{io}} = K \times \tfrac{1}{2}\rho_a|U_o|U_o \tag{27}$$

These are expected results that can also be obtained from application of continuity and energy equations for the steady flow situation.

The coupled equations (1), (3), (13), (22), and (23) constitute the synthetic jet actuator model, which relates the input force $F(t)$ to the oscillating wall displacement $x_w(t)$, cavity internal pressure $p_i(t)$, and the actuator output or orifice velocity $U(t)$. Because Eqs. (22) and (23) are nonlinear, a numerical solution scheme has to be employed to solve for these variables for a given forcing voltage $v(t)$ or oscillating force $F(t)$. In this study, a fourth-order Runge–Kutta scheme [28] was employed. To implement this numerical solution procedure, the set of equations are rewritten as follows:

$$p_i = \dot{p}_i\,\mathrm{d}t, \qquad x_w = \dot{x}_w\,\mathrm{d}t, \qquad \dot{x}_w = \ddot{x}_w\,\mathrm{d}t, \qquad U = \dot{U}\,\mathrm{d}t \tag{28a}$$

$$\dot{p}_i = \frac{\gamma A_w P_o}{V_o}\dot{x}_w - \frac{\gamma A_o P_o}{V_o}U \tag{28b}$$

$$\dot{U} = \frac{p_i}{\rho l_e}\dot{x}_w - \frac{K}{2l_e}|U|U \tag{28c}$$

$$\ddot{x}_w = \frac{F}{m_{\text{wt}}}\dot{x}_w - \frac{p_i A_w}{m_{\text{wt}}} 2\zeta_w \omega_w \dot{x}_w - \omega_w^2 x_w \tag{28d}$$

An appropriate choice of time-step Δt is made based on the frequency of the forcing function and the solution is then advanced with zero initial conditions.

III. Model Validation

For validation of the present model, we consider the two piezoelectric-driven synthetic jet actuators (1 and 2) studied by Gallas et al. [15–17], for which physical and experimental data are available and which are summarized here in Table 2. Because input to the present model is a sinusoidal force on the diaphragm, the amplitude of this force is estimated using data from [15–17] in Table 2. Using the effective acoustic piezoelectric coefficient D_a, a volume displacement magnitude ΔV is first calculated for the given forcing voltage amplitude. By equating this to an equivalent volume displacement $\Delta V = A_w x_w$ in the present model, a displacement amplitude results that, combined with the wall stiffness, yields the force amplitudes of 0.574 and 0.401 N for cases 1 and 2, respectively.

Figures 4–6 compare the maximum orifice velocity predicted by the present model with those from the experiment and LEM model of Gallas et al. [15–17], for cases 1 and 2, respectively. Figure 4 shows that there is good agreement between the present model and experiment, except in the midfrequency region, in which the model overpredicts the maximum velocities somewhat. This is similar to the prediction of the LEM model. The LEM model, on the other hand, underpredicts the first resonant peak, which clearly relates to the choice of a higher loss coefficient of 1.0, compared with a value of 0.78 used in the present study. The value $K = 0.78$ was chosen because it gave a good match to the peak response. The resonance frequencies of 953 and 2184 Hz predicted by the model agree quite well with experimental data.

The sensitivity to the orifice loss coefficient was investigated by computing responses for a range of K values. The results are illustrated in Fig. 5, which shows that the peak responses at both

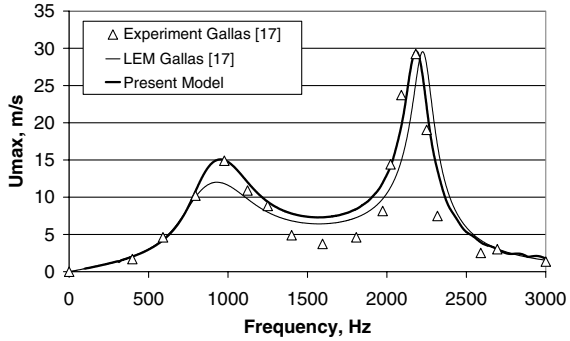

Fig. 4 Comparisons between the model, experiment, and the LEM [17] for case 1.

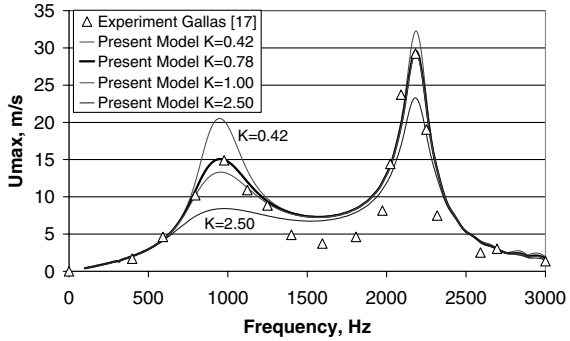

Fig. 5 Sensitivity of the actuator output to the orifice loss coefficient K for case 1.

resonances are indeed sensitive to the choice of the orifice loss coefficient K. The orifice loss coefficient K directly determines the losses and thus represents damping in the system. Consequently, the peak response of the actuator about the resonance frequencies is sensitive to K. The analysis presented here suggests that K will be somewhat higher than the steady sudden-contraction loss coefficient of 0.42, but significantly lower than that for a sharp-edged orifice in steady flow. The data here suggest that a reasonable range for K values would be between 0.42 and 1.0. Further studies are, however, warranted to be able to accurately predict this important parameter.

In Fig. 6 for case 2, agreement between the present model and experiment is good again. In this case, although the model overpredicts the maximum velocities somewhat near the highly

Table 2 Properties of piezoelectric-driven synthetic jet actuators of Gallas et al. [15–17]

Component	Property	Case 1	Case 2
Brass shim	Density, kg/m^3	8700	8700
	Thickness, mm	0.20	0.10
	Diameter, mm	23.5	37.0
Piezoceramic	Density, kg/m^3	7700	7700
	Thickness, mm	0.11	0.10
	Diameter, mm	20.5	25.0
Diaphragm	Compliance, s$^2 \cdot$ m^4/kg	6.53×10^{-13}	2.23×10^{-11}
	Acoustic mass, kg/m^4	8.15×10^{3}	2.43×10^{3}
	Acoustic piezoelec coeff D_a, m^3/V	5.53×10^{-11}	4.32×10^{-10}
	Mechanical damping ratio	0.03	0.03
	Natural frequency, Hz	2114	632
Cavity	Volume, m^3	2.5×10^{-6}	5.0×10^{-6}
	Equivalent cylindrical diameter, mm	23.5	37.0
	Equivalent cylindrical length, mm	5.76	4.65
Orifice	Diameter, mm	1.65	0.84
	Length, mm	1.65	0.84
	Effective loss coefficient	0.78	0.78
	Inertia coefficient	0.705	0.86
	Helmholtz frequency, Hz	977	473
Forcing	Voltage amplitude, V	25	25
	Force amplitude, N	0.574	0.401

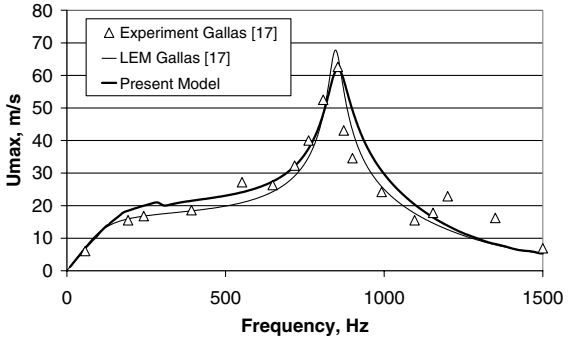

Fig. 6 Comparisons between the model, experiment and the LEM [17] for case 2.

damped first resonance, it nevertheless gives a good prediction of the maximum velocity at the resonant peak at 854 Hz, with $K = 0.78$. The LEM model with a loss coefficient of 1.0 overpredicts the maximum velocity in this case. That this is the case is not surprising, because the loss and other orifice coefficients used in the present and past studies are taken as constant values, whereas the oscillatory nature of the orifice flow would mean that these are, in fact, not constant. Clearly, further studies are required to obtain accurate representations for these coefficients. Notwithstanding this, the agreement between the present model and experiment is nevertheless good, which allows the new model to be used in the analysis of the performance of the actuator to important parameters.

Figure 7 displays the maximum diaphragm displacement and velocity, internal pressure, and the orifice velocity calculated using the present model for case 1. It shows that large-amplitude oscillations in internal pressure are obtained within a synthetic jet actuator, and they are most enhanced at the two resonant frequencies. Further validation of the new model is provided from a comparison of the calculated phase angles in Fig. 8, with experimentally measured data of Gallas et al. [18]. At the very low frequencies, the model shows that the phase angle between the diaphragm velocity and the orifice flow velocity, $\phi_{V_w\text{-}U}$, is near 0 deg (i.e., the two

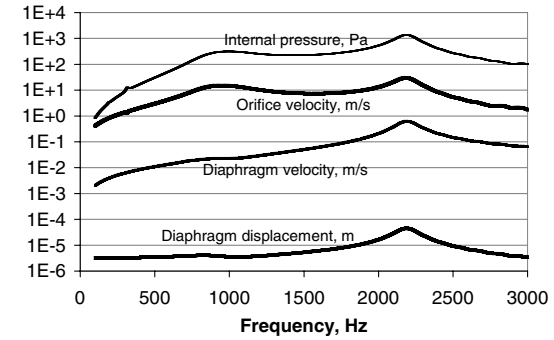

Fig. 7 Calculated maximum diaphragm displacement and velocity, internal pressure and the orifice velocity for case 1 (on a logarithmic scale).

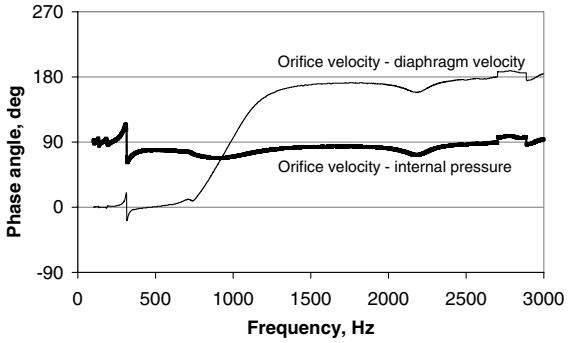

Fig. 8 Calculated phase angles for case 1.

velocities are very nearly in phase), indicating that the flow is incompressible. Near the first resonant peak, however, the flow becomes compressible, as indicated by an increase in the phase angle $\phi_{V_w\text{-}U}$ from zero, at around 750 Hz, to nearly 90 deg. This relates to the relative magnitudes of the inertia and damping forces. In contrast, the phase angle between the internal pressure and the orifice velocity, $\phi_{P_i\text{-}U}$, is nearly constant around 90 deg over the entire frequency range. These findings are qualitatively and quantitatively in agreement with the measurements of Gallas et al. [18].

A further observation in Figs. 7 and 8 is that although the phase angle $\phi_{V_w\text{-}U}$ is approximately zero at low frequencies, it is approximately 180 deg at the higher frequencies and, in particular, around the second resonant peak. This clearly implies that the diaphragm and orifice flow movements are in phase or in harmony with each other at the low frequencies. At the second resonance mode, however, $\phi_{V_w\text{-}U} \approx 180$ deg clearly implies that the diaphragm and orifice flow movements are out of phase. This behavior is very similar to that of a two-degree-of-freedom mechanical system consisting of two masses, two springs, and two dash pots connected in series.

The implication of these results is that the behavior of the air in the actuator cavity is compressible not only around the Helmholtz frequency, but more so at all frequencies beyond the Helmholtz frequency. This is contrary to the general belief that compressibility may be important only when the actuator is driven around the Helmholtz resonance frequency of the cavity. This important result has significant implications for CFD modeling of synthetic jet actuators, especially when actuators are most efficiently driven at either resonance frequency.

IV. Further Analysis Using the Model

The model was used to analyze the performance of the actuator and its sensitivity to changes of important design parameters. As an example, the influence of cavity volume on the maximum orifice flow velocity for case 1 is shown in Fig. 9. The trends are similar to the LEM results of Gallas et al. [18], showing decrease in Helmholtz resonance and thus the first resonance frequency with increasing volume. This is accompanied by decreased response as the first and second resonance peaks become smaller with larger volume. A solution was also obtained for 21% of the nominal volume for case 1, at which the Helmholtz resonance frequency is exactly equal to the diaphragm resonance frequency of 2114 Hz. Although the maximum output velocity in this situation is slightly lower than that obtained for a 50% volume, a broadband response is nevertheless evident. The actuator output is relatively large over a wide frequency range, and such a condition may be desirable when the operating conditions might drift or are not exactly determinable during design.

The influence of the diaphragm resonance frequency, physically achieved by adding mass, on the actuator output is shown in Fig. 10. Two solutions were obtained, corresponding to increased diaphragm mass relative to case 1 (see Table 2), one of which was "tuned" so that the diaphragm natural frequency exactly equaled the Helmholtz resonance frequency of 977 Hz. Again, the actuator output is seen to

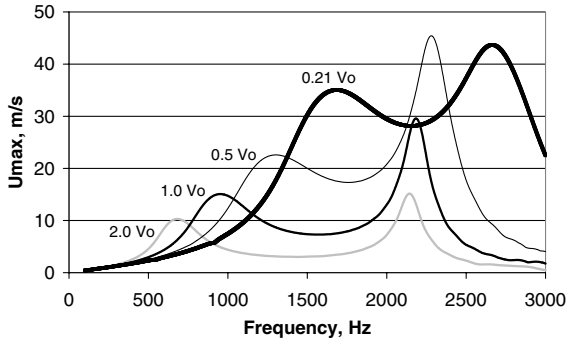

Fig. 9 Model predictions for varying cavity volume (case 1).

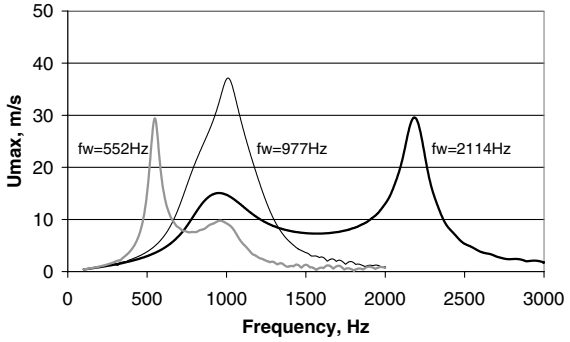

Fig. 10 Model predictions for varying diaphragm mass (case 1).

be maximized when the two resonance frequencies are brought close to each other.

V. Conclusions

An analytical model for a synthetic jet actuator based on the laws of fluid dynamics was developed and validated against experimental data in the published literature. The model is able to predict the performance and sensitivity of the actuator, defined by the orifice flow velocity, to changes of important design parameters and inputs. It is also able to predict actuator cavity pressure variations and the phase relationships between the actuator diaphragm movements and the orifice velocity. The model and analysis based on it provide valuable insights into the behavior of synthetic jet actuators and reveals that the behavior of the air in the actuator cavity is compressible at all frequencies from around the Helmholtz frequency and beyond.

Acknowledgment

The grant support from the Research Committee of the University of Auckland is gratefully acknowledged.

References

[1] James, R. D., Jacobs, J. W., and Glezer, A., "A Round Turbulent Jet Produced by an Oscillating Diaphragm," *Physics of Fluids*, Vol. 8, No. 9, 1996, pp. 2484–2495.

[2] Smith, B. L., and Glezer, A., "The Formation and Evolution of Synthetic Jets," *Physics of Fluids*, Vol. 10, No. 9, 1998, pp. 2281–2297.

[3] Glezer, A., and Amitay, M., "Synthetic Jets," *Annual Review of Fluid Mechanics*, Vol. 34, 2002, pp. 503–529.

[4] Smith, D., and Glezer, A., "Vectoring and Small-Scale Motions Effected in Free Shear Flows Using Synthetic Jet Actuators," AIAA Paper 98-0209, 1998.

[5] Davis, S. A., and Glezer, A., "Mixing Control of Fuel Jets Using Synthetic Jet Technology," AIAA Paper 99-0447, 1999.

[6] Crook, A., Sadri, A. M., and Wood, N. J., "The Development and Implementation of Synthetic Jets for the Control of Separated Flow," AIAA Paper 99-3176, 1999.

[7] Smith, D. R., "Interaction of a Synthetic Jet with a Crossflow Boundary Layer," *AIAA Journal*, Vol. 40, No. 11, 2002, pp. 2277–2288.

[8] Benchiekh, M., Bera, J-C., Michard, M., and Sunyach, M., "Contróle Par Jet Pulse de L'Écoulement Dans un Divergent Court à Grand Angle," *Mécanique des Fluides*, Série 2b, Vol. 328, No. 10, Comptes Rendus de l'Academie de Science, Paris, 2000, pp. 749–756.

[9] Amitay, M., Pitt, D., Kibens, V., Parekh, D., and Glezer, A., "Control of Internal Flow Separation Using Synthetic Jet Actuators," AIAA Paper 2000-0903, 2000.

[10] Amon, C. H., Murthy, J., Yao, S. C., Narumanchi, S., Wu, C., and Hsieh, C., "MEMS Enabled Thermal Management of High Heat Flux Devices (EDIFICE)," *Experimental Thermal and Fluid Science*, Vol. 25, No. 5, 2001, pp. 231–242.

[11] Traničěk, Z., and Tesař, V., "Annular Synthetic Jet Used for Impinging Flow Mass Transfer," *International Journal of Heat and Mass Transfer*, Vol. 46, No. 17, 2003, pp. 3291–3297.

[12] Mallinson, S. G., Hong, G., and Reizes, J. A., "Some Characteristics of Synthetic Jets," AIAA Paper 99-3651, June 1999.

[13] Guy, Y., T. McLaughlin, E., and Albertson, J. A., "Velocity Measurements in a Synthetic Jet," AIAA Paper 2000-0118, 2000.

[14] Guy, Y., McLaughlin, T. E., and Albertson, J. A., "Effect of Geometric Parameters on the Velocity Output of a Synthetic Jet Actuator," AIAA Paper 2002-0126, 2002.

[15] Gallas, Q., Mathew, J., Kaysap, A., Holman, R., Nishida, T., Carroll, B., Sheplak, M., and Cattafesta, L., "Lumped Element Modeling of Piezoelectric- Driven Synthetic Jet Actuators," AIAA Paper 2002-0125, Jan. 2002.

[16] Gallas, Q., Holman, R., Nishida, T., Carrol, B., Sheplak, M., and Cattafesta, L., "Lumped Element Modeling of Piezoelectric- Driven Synthetic Jet Actuators," *AIAA Journal*, Vol. 41, No. 2, 2003, pp. 240–247.

[17] Gallas, Q., Wang, G., Papila, M., Sheplak, M., and Cattafesta, L., "Optimisation of Synthetic Jet Actuators," AIAA Paper 2003-0635, Jan. 2003.

[18] Gallas, Q., Holman, R., Raju, R., Mittal, R., Sheplak, M., and Cattafesta, L., "Low Dimensional Modeling of Zero-Net Mass-Flux Actuators," AIAA Paper 2004-2413, July 2004.

[19] Kinsler, L. E., Frey, A. R., Coppens, A. B., and Sanders, J. V., *Fundamentals Of Acoustics*, 4th ed., Wiley, New York, 2000, pp. 184–187.

[20] Hall, D. E., *Basic Acoustics*, Krieger, Malabar, FL, 1987, pp. 107–109, 235–243.

[21] Rathnasingham, R., and Breuer, K. S., "Coupled Fluid-Structural Characteristics of Actuators for Flow Control," *AIAA Journal*, Vol. 35, No. 5, 1997, pp. 832–837.

[22] Etheridge, D. W., "Nondimensional Methods for Natural Ventilation," *Building and Environment*, Vol. 37, No. 11, 2002, pp. 1057–1072.

[23] Sharma, R. N., and Richards, P. J., "Computational Modeling of the Transient Response of Building Internal Pressure to a Sudden Opening," *Journal of Wind Engineering & Industrial Aerodynamics*, Vol. 72, No. 1, 1997, pp. 149–161.

[24] Vickery, B. J., "Internal Pressures and Interactions with the Building Envelope," *Journal of Wind Engineering & Industrial Aerodynamics*, Vol. 53, 1994, pp. 125–144.

[25] Sharma, R. N., and Richards, P. J., "Computational Modeling in the Prediction of Building Internal Pressure Gain Functions," *Journal of Wind Engineering & Industrial Aerodynamics*, Vols. 67–68, Apr.–June 1997, pp. 815–825.

[26] White, F. M., *Fluid Mechanics*, 4th ed., McGraw–Hill, New York, 1999, pp. 371–373.

[27] White, F. M., *Viscous Fluid Flow*, McGraw–Hill, New York, 1974, pp. 143–148.

[28] Press, W. H., Flannery, B. P., Teukolsky, S. A., and Vetterling, W. T., *Numerical Recipes in C: The Art of Scientific Computing*, 2nd ed., Cambridge Univ. Press, New York, 1992, pp. 710–714.

A. Tumin
Associate Editor